Available online at www.sciencedirect.com
SCIENCE DIRECT
Journal of Catalysis 229 (2005) 114–118
JOURNAL OF CATALYSIS
www.elsevier.com/locate/jcat

Magnetic nanocomposite catalysts with high activity and selectivity for selective hydrogenation of *ortho*-chloronitrobenzene

Junling Zhang [a], Yuan Wang [a,*], Hua Ji [a], Yongge Wei [a], Nianzu Wu [a], Bojun Zuo [b], Qilong Wang [b]

[a] *State Key Laboratory for Structural Chemistry of Unstable and Stable Species, College of Chemistry and Molecular Engineering, Peking University, Beijing 100871, P.R. China*

[b] *Department of Chemistry, Shandong University, Jinan 250100, P.R. China*

Received 20 August 2004; revised 30 September 2004; accepted 30 September 2004

Available online 26 November 2004

Abstract

We report the preparation and characterization of a Pt/γ-Fe_2O_3 nanocomposite catalyst and its novel catalytic properties for the selective hydrogenation of *ortho*-chloronitrobenzene (*o*-CNB). The catalytic hydrodechlorination of the hydrogenation product *ortho*-chloroaniline (*o*-CAN) over the catalyst was fully suppressed for the first time at complete conversion of *o*-CNB. The nanocomposite catalyst also exhibited excellent catalytic activity and stability for the reaction of interest, suggesting that it may be suitable for industrial application. The magnetic property of the Pt/γ-Fe_2O_3 nanocomposite provided a convenient route for separating the catalyst from the reaction system in an applied magnetic field.

Keywords: Pt nanoclusters; Nanocomposite catalyst; *ortho*-Chloronitrobenzene Hydrogenation; Magnetic separation; Dehalogenation

1. Introduction

Aromatic chloroamines are important intermediates in the chemistry of dyes, drugs, herbicides, and pesticides. At present these compounds are produced by hydrogenation of the corresponding chloronitro compounds over metal catalysts [1]. Selective hydrogenation of chloronitrobenzene (CNB) to the corresponding chloroaniline (CAN) has been well studied over the Pt and Pt-alloy catalysts, which have high catalytic activity and a relatively low catalytic hydrodechlorination rate [2–7]. To solve the problem of the catalytic hydrodechlorination of CAN, many effective strategies have been developed that involve the alloying of Pt with other metals [4,5] and the modification of Pt particles with sub-oxide species, such as TiO_x [7], or with metal cations [3]. However, the hydrodechlorination of the products as a defect of this process could not be avoided completely over the Pt-based catalysts reported previously, especially for the complete conversion of the substrates.

Metal nanoclusters are very promising building blocks in the preparation of heterogeneous catalysts with a controllable structure, which can be synthesized in a solvent and then deposited on a support without obvious aggregation [8–14]. We reported a Ru/SnO_2 nanocomposite catalyst, prepared simply by capture of the "unprotected" Ru nanoclusters (stabilized with ethylene glycol and simple ions) on SnO_2 colloidal particles via electrostatic interaction, followed by gelation of the obtained complex sol through adjustment of its pH [15]. Compared with other Ru-based catalysts, the Ru/SnO_2 nanocomposite catalysts exhibited high catalytic activity for the *ortho*-chloronitrobenzene (*o*-CNB) hydrogenation reaction and low activity for the dechlorination of *o*-CAN due to a synergic effect between the Ru metal nanoclusters and the inorganic support. Here we report the preparation of a magnetic Pt/γ-Fe_2O_3 nanocomposite cata-

* Corresponding author. Fax: +86-10-6276-5769.
E-mail address: wangy@pku.edu.cn (Y. Wang).

0021-9517/$ – see front matter
doi:10.1016/j.jcat.2004.09.029

lyst by means of this strategy, but with a few modifications, and its excellent catalytic properties for the selective hydrogenation of *o*-CNB. Over this nanocomposite catalyst, the hydrodechlorination of the product *o*-CAN was completely suppressed at an *o*-CNB conversion of 100%, and the high catalytic activity of the Pt nanoclusters was essentially maintained. The ferromagnetic property of the nanocomposite catalyst made possible the convenient separation of the nanocomposite catalyst from the reaction system in an applied magnetic field.

2. Experimental

The "unprotected" Pt nanoclusters (about 2.5 nm in diameter), stabilized with simple ions and ethylene glycol, and PVP-protected Pt colloids of the same Pt particle size were prepared according to a method reported previously [16]. To prepare a colloidal solution of iron oxides, an aqueous solution of ammonia (10%) was added to a solution of $FeCl_3$ (4%) in 100 ml of water to adjust the pH to about 7.5, producing a precipitate that was separated by a filter, washed with water, and peptized in 30 ml of aqueous solution of $FeCl_3$ (1.2%), resulting in a transparent colloidal solution of ferric hydroxide. The Pt/γ-Fe_2O_3 nanocomposite catalyst was prepared by heating of a mixture of the "unprotected" Pt colloid and the ferric hydroxide colloid at the required ratio. In a typical experiment, the mixture was heated in a Teflon-lined autoclave at 353 K for 3 days. A magnetic precipitate was produced, which was separated by centrifugation, and dried at 353 K to give a brownish red solid (Pt/γ-Fe_2O_3).

A classical heterogeneous Pt/Fe_3O_4 catalyst with 1 wt% Pt loading was prepared by incipient wetness impregnation with the use of $H_2PtCl_6 \cdot 6H_2O$ and a prepared iron oxide support as the precursors. The iron oxide support was obtained by a method similar to that used to prepare the Pt/γ-Fe_2O_3 nanocomposite, but without the addition of the Pt colloid. The catalyst was calcined at 573 K for 2 h and reduced with hydrogen at 523 K for 3 h.

The specific surface area and metal Pt dispersion of the catalysts were measured on a Micromeritics ASAP 2010 M + C instrument. XRD patterns were recorded with a Rigaku Dmax 2500 diffractometer with Cu radiation at 40 kV and 300 mA. STEM images were taken on a Philips Tecnai F30 scanning transmission electron microscope equipped with a high-angle–annular dark-field (HAADF) detector. The XPS measurements were made with an Axis Ultra photoelectron spectrometer. The saturation magnetization was measured with an AGM MicroMag 2900 instrument at room temperature.

Hydrogenation of *o*-CNB under atmospheric pressure was performed in a 50-ml reactor at 333 K. Prior to the reaction, the catalyst, dispersed in 25 ml of methanol, was activated in hydrogen for 30 min. Then 1.27 mmol of *o*-CNB was added to the reaction system to start the reaction. The reactions were followed by hydrogen uptake under atmospheric pressure. The reaction products were analyzed on a Beifen 3420 gas chromatograph equipped with a FID detector and a DC-710 packed column.

3. Results and discussion

The "unprotected" Pt, Rh, and Ru metal nanoclusters, with a small particle size and narrow size distribution, and stabilized by ethylene glycol and simple anions [16], are very tractable for preparing nanocomposite catalysts; they can easily be prepared on a large scale and can be assembled with different metal oxide nanoparticles. The stabilizers in these metal colloids can be removed easily during the immobilization process, resulting in the direct contact of the metal nanoclusters with the support framework formed by the gelation of the metal oxide nanoparticles. This is important for the modulation of the catalytic properties of the catalysts through electron interaction between the metal nanoparticles and the support or by the function of the surface species.

The Pt/γ-Fe_2O_3 nanocomposite catalyst was prepared by capture of the synthesized "unprotected" Pt nanoclusters on the colloidal particles of ferric hydroxides via electrostatic interaction, followed by heating of the mixture in an autoclave at 353 K. Fig. 1A shows the Z-contrast STEM image of the Pt/γ-Fe_2O_3 nanocomposite catalyst. Combined EDX analysis (Fig. 1B), using an electron beam 0.8 nm in diameter to scan along the line marked in Fig. 1A, revealed that the signal of Pt was detectable at the small, brightest spots; iron, on the other hand, was present in the bright area. Therefore, the brightest cores in the bright area are the images of the Pt nanoparticles.

The crystal structure of the magnetic Pt/γ-Fe_2O_3 nanocomposite catalyst was characterized by powder X-ray diffraction (XRD). Compared with the data of maghemite, magnetite, and hematite, the five strongest diffraction peaks with $d = 2.5198$, 1.4772, 2.9588, 1.6081, and 2.0906, respectively, in the XRD pattern of the Pt/γ-Fe_2O_3 nanocomposite match those in the pattern of maghemite [17]. According to the widths of the peaks, the average diameter of the maghemite crystal grains in the Pt/γ-Fe_2O_3 nanocomposite catalyst is about 15 nm, as calculated with the Scherrer equation. The formation of the maghemite phase rather than magnetite in the magnetic Pt/γ-Fe_2O_3 nanocomposite catalyst was further confirmed by chemical analysis, XPS, and Raman spectra investigations, which will be reported elsewhere. Diffraction signals of Pt nanoparticles in the Pt/γ-Fe_2O_3 nanocomposite catalyst were not detected because of the low metal content and small particle size.

The physical properties of the magnetic Pt/γ-Fe_2O_3 nanocomposite catalyst are reported in Table 1, as are the physical properties of a PVP-protected Pt catalyst with the same Pt nanoparticles and a classically prepared Pt/Fe_3O_4 catalyst for comparison (see Section 2). The average diameters of the Pt nanoparticles in the Pt/γ-Fe_2O_3 nanocomposite catalyst, measured by STEM and H_2 chemisorption, are 2.6

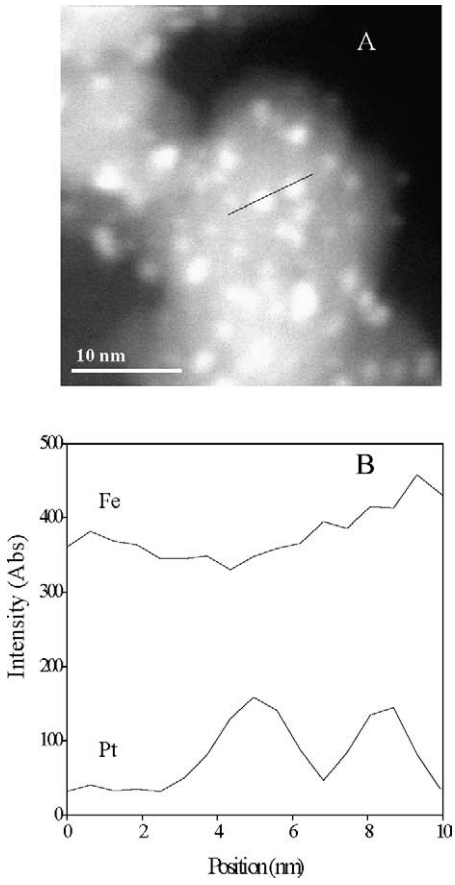

Fig. 1. (A) HAADF STEM image of Pt nanoparticles captured on the surface of iron oxides particles. (B) EDX patterns of the complex nanoparticles measured using an electron beam of 0.8 nm in diameter.

and 2.4 nm, respectively, which agree with the diameters of the original Pt nanoclusters in the Pt colloidal solution. This suggests that Pt nanoclusters are well dispersed in the matrix network of the Fe_2O_3 support without obvious aggregation.

As shown in Table 1, the binding energy of the Pt $4f_{7/2}$ level in the prepared PVP-protected Pt nanoparticles is very close to that of bulk Pt metal (71.0 eV). This suggests that the size-dependent effect on the electron-binding energies of Pt nanoparticles, derived from the final state relaxation [18], becomes negligible at a size of 2.5 nm. The binding energy of the Pt $4f_{7/2}$ level in both Pt-supported catalysts was 71.5 eV, which are 0.6 eV higher than that of the PVP-protected Pt nanoparticles. This reveals the electron transfer, which occurs from the Pt particles to the iron oxide supports, and the electron-deficient state of the Pt nanoparticles in the present heterogeneous catalysts.

Table 2 lists the catalytic properties over the Pt/γ-Fe_2O_3 nanocomposite, Pt/Fe_3O_4, and the PVP-protected Pt colloid catalysts for the hydrogenation of *o*-CNB. The PVP-Pt colloid catalyst was the most active catalyst of the examined catalysts, with a hydrogenation rate of 59.0 $mmol_{o\text{-CNB}}/(mol_{Pt}\,s)$. However, the selectivity of *o*-CAN over this Pt colloidal catalyst was only 45% at the complete conversion of *o*-CNB. Over the Pt/γ-Fe_2O_3 nanocomposite catalyst, the catalytic hydrogenation rate of *o*-CNB was 67% of that over the PVP-Pt colloidal catalyst, whereas the *o*-CAN selectivity was higher than 99.9%. We did not detect any by-products derived from the hydrodechlorination over the nanocomposite catalyst, even when the reaction time was extended by 9 h after *o*-CNB was exhausted. Thus, the hydrodechlorination of the product *o*-CAN was completely suppressed, while the catalytic activity of the Pt nanoclusters for the hydrogenation of *o*-CNB was maintained. The Pt/γ-Fe_2O_3 nanocomposite catalyst was more active than the classically prepared Pt/Fe_3O_4 catalyst, because the Pt particles in the Pt/γ-Fe_2O_3 nanocomposite catalyst were much smaller than those in the Pt/Fe_3O_4 catalyst. However, we found no intrinsic difference in the specific rate (turnover frequency over per surface Pt atom) and the catalytic selectivity between the Pt/Fe_3O_4 catalyst (0.10 s^{-1}) and Pt/γ-Fe_2O_3 nanocomposite catalyst (0.09 s^{-1}). This differs from previously reported results, which showed that the specific rate and the product selectivity for the catalytic hydrogenation of *para*-chloronitrobenzene over the Pt/Al_2O_3 catalysts depended strongly on the Pt particle size [2].

Coq et al. studied the influence of supports on the catalytic properties of Pt-supported catalysts for the hydrogenation of *p*-CNB. Over a Pt/TiO_2 catalyst with a strong metal/support interaction (SMSI), a selectivity of 99.3% for *p*-CAN was obtained at 99.7% conversion of *p*-CNB [7]. However, the intrinsic rate (TOF) of *p*-CAN hydrodechlorination over the Pt/TiO_2 catalyst was twice as high as that over the Pt/Al_2O_3 catalyst, that is, the Pt/TiO_2 catalyst accelerated not only the hydrogenation of CNB, but also the

Table 1
Physical properties of the as-prepared Pt catalysts

Catalysts	S_{BET}[a] (m^2/g)	d_{Pt} (nm)			Dispersion[c] (%)	Pt $4f_{7/2}$[d] (eV)	M_s[e] (emu/g)
		H_2 chemisorption	TEM	XRD[b]			
PVP-Pt	–	–	2.5	–	–	70.9	–
Pt/Fe_3O_4	11	19.6	12.5	16.0	5.1	71.5	96.0
Pt/γ-Fe_2O_3	22	2.4	2.6	–	42.5	71.5	59.8

[a] The specific surface area determined by N_2 adsorption at 77 K.
[b] Average crystal grain size of Pt particles, determined from the peak width of the Pt(111) XRD signal.
[c] Metal Pt dispersions determined by H_2 chemisorption at 323 K.
[d] The signals were calibrated by assigning a value of 284.8 eV to the C 1s peak of the contaminant carbon.
[e] Saturation magnetization of the samples measured at room temperature.

Table 2
Catalytic properties for the hydrogenation of *o*-CNB over the as-prepared Pt catalysts[a]

Catalysts [b]	Pt in catalyst (mmol)	*o*-CNB (mmol)	Pressure (MPa)	Reaction time (min)	Conversion[c] (%)	Rate[d]	Selectivity (mol%)	
							o-CAN	AN
Pt-PVP	1.02×10^{-2}	1.27	0.1	35	100	5.9×10^{-2}	45.3	43.4
Pt/Fe_3O_4	1.02×10^{-2}	1.27	0.1	392	100	5.3×10^{-3}	> 99.9	0.0
Pt/γ-Fe_2O_3	1.02×10^{-2}	1.27	0.1	52	100	4.0×10^{-2}	> 99.9	0.0
Pt/γ-Fe_2O_3	1.02×10^{-2}	13.0	0.1	95	100	2.2×10^{-1}	> 99.9	0.0
Pt/γ-Fe_2O_3	2.55×10^{-3}	13.0	1.0	10	49.0	4.2	> 99.9	0.0
Pt/γ-Fe_2O_3	2.55×10^{-3}	13.0	2.0	10	76.0	6.5	> 99.9	0.0
Pt/γ-Fe_2O_3	2.55×10^{-3}	13.0	4.0	10	89.4	7.6	> 99.9	0.0
Pt/γ-Fe_2O_3	2.55×10^{-3}	13.0	4.0	20	100	–	> 99.9	0.0
Pt/γ-Fe_2O_3	2.55×10^{-3}	13.0	4.0	240	100	–	> 99.9	0.0

[a] Reaction conditions: solvent, 25 ml methanol; temperature, 333 K. The reaction system was stirred with a magnetic stirrer.
[b] Pt content: Pt/γ-Fe_2O_3 and Pt/Fe_3O_4, 1 wt% Pt.
[c] Conversion of *o*-CNB.
[d] Average rate of *o*-CNB hydrogenation ($mol_{o\text{-CNB}}/(mol_{Pt}\ s)$).

hydrogenolysis of the C–Cl bond in CAN. Therefore, the hydrodechlorination of CAN was unavoidable over the Pt/TiO_2 catalyst, and better selectivity of CAN was possible only before the complete conversion of CNB.

From the experimental results, we conclude that the high selectivity of *o*-CAN over the Pt/γ-Fe_2O_3 nanocomposite catalyst is derived from the suppression of *o*-CAN hydrodechlorination, which is of the utmost importance if pure products are to be obtained effectively in the selective hydrogenation of aromatic chloronitro compounds. This advantage of the catalyst is clearly shown by the catalytic properties under the elevated H_2 pressure (Table 2). Over the Pt/γ-Fe_2O_3 nanocomposite catalyst, the hydrogenation rate of *o*-CNB was 34 times higher when the H_2 pressure was increased from 0.1 to 4 MPa at 333 K. No obvious loss of catalytic selectivity was observed, even when all of the *o*-CNB was exhausted under 4 MPa and at 333 K. To the best of our knowledge, this excellent catalytic property for the hydrogenation of *o*-CNB over Pt-based catalysts has not been reported elsewhere.

Aramendia et al. and Coq et al. proposed a radical mechanism for the hydrogenation of substituted nitroaromatics over Pt/SiO_2–$AlPO_4$ and Pt/Al_2O_3 catalysts, respectively [2,19]. For the mechanism in the hydrodehalogenation reaction of aromatic halides, most researchers agree that there is an electrophilic attack of cleaved hydrogen on the adsorbed aromatic halides [7,20,21]. Based on the XPS data (Table 1), we believe that the electron-deficient state of the Pt particles, supported on the iron oxide supports, would weaken the extent of electron feedback from the Pt particles to the aromatic ring in *o*-CAN, which would further suppress the hydrodechlorination of *o*-CAN.

Liu et al. reported the influence of metal ions, added as their chlorides, on the catalytic properties over a PVP-protected Pt colloid catalyst for the hydrogenation of *o*-CNB, and found that Ni^{2+} and Fe^{3+} ions had a promotion effect on the selectivity of *o*-CAN [3]. In a recent paper, we suggested that the vacancies at the surface of SnO_2 nanoparticles in a Ru/SnO_2 nanocomposite catalyst may be important in depressing the hydrodechlorination reaction of *o*-CAN [15]. Therefore, we deduced that the vacancies, that is, the coordinatively unsaturated Fe^{3+} or Fe^{2+} species, at the surface of iron oxide nanoparticles in the Pt/γ-Fe_2O_3 catalyst may also play a role in the high catalytic selectivity of the coordination with the amino group of *o*-CAN.

The Pt/γ-Fe_2O_3 catalyst is robust; its ferromagnetic property is it useful for separating the catalyst from the reaction system in an applied magnetic field. Upon completion of *o*-CNB hydrogenation, the Pt/γ-Fe_2O_3 catalyst was separated from the dispersion by attraction of the catalyst particles to a magnet and, thus, removing them from the solution. After washing with methanol to remove the adsorbed species, the recovered catalyst was reused in the next cycle of the reaction. The recovered catalyst exhibited the same selectivity for *o*-CAN without an obvious loss of catalytic activity over five cycles. The stability of the catalyst was also evaluated under 4 MPa of hydrogen at 333 K; a turnover number of more than 100,000 and a selectivity higher than 99.9% of *o*-CAN was achieved.

4. Conclusion

The prepared Pt/γ-Fe_2O_3 nanocomposite catalyst exhibited good activity and very high selectivity for the selective hydrogenation of *o*-CNB to *o*-CAN. The hydrodechlorination of the product *o*-CAN was hindered over this new catalyst, even after the complete conversion of *o*-CNB. From 0.1 to 4 MPa, the nanocomposite catalyst worked perfectly, with an extremely high selectivity of *o*-CAN and excellent catalytic activity. The catalyst was also very stable, and its ferromagnetic property proved convenient for separating the catalyst from the reaction system in an applied magnetic field. The results described here show that the Pt/γ-Fe_2O_3 nanocomposite is a promising catalyst for industrial application.

Acknowledgments

This work was jointly supported by the NSFC (project 29925308, and 90206011), Chinese Ministry of Education (project 99000) and the Chinese Ministry of Science and Technology (project G2000077503).

References

[1] V. Kratky, M. Kralik, M. Mecarova, M. Stolcova, L. Zalibera, M. Hronec, Applied Catalysis A: General 235 (2002) 225, and references therein.
[2] B. Coq, A. Tajani, F. Figuéras, J. Mol. Catal. A 68 (1991) 331.
[3] X. Yang, H. Liu, Appl. Catal. A 164 (1997) 197.
[4] X. Han, R. Zhou, X. Zheng, H. Jiang, J. Mol. Catal. A 193 (2003) 103.
[5] B. Coq, A. Tijani, F. Figuéras, J. Mol. Catal. 71 (1992) 317.
[6] X.X. Han, R.X. Zhou, G.H. Lai, B.H. Yue, X.M. Zheng, J. Mol. Catal. A 209 (2004) 83.
[7] B. Coq, A. Tijani, R. Dutartre, F. Figuéras, J. Mol. Catal. A 79 (1993) 253.
[8] J. Niederer, A. Arnold, W. Hölderich, B. Spliethof, B. Tesche, M. Reetz, H. Bönnemann, Topics in Catal. 18 (3–4) (2002) 265.
[9] M. Reetz, M. Dugal, Catal. Lett. 58 (1999) 207.
[10] R. Raja, T. Khimyak, J. Thomas, S. Hermans, B. Johnson, Angew. Chem. Int. Ed. 40 (24) (2001) 4638.
[11] A. Martino, A. Sault, J. Kawola, E. Boespflug, M. Phillips, J. Catal. 187 (1999) 30.
[12] A. Miyazaki, I. Balint, K. Aika, Y. Nakano, J. Catal. 204 (2001) 364.
[13] W. Li, W. Zhou, H. Li, Z. Zhou, B. Zhou, G. Sun, Q. Xin, Electrochimica Acta 49 (2004) 1045.
[14] S. Mao, G. Mao, Supported nanoparticle catalyst, USA Patent, US 2003/0104936 A1, June 5, 2003.
[15] B. Zuo, Y. Wang, Q. Wang, J. Zhang, N. Wu, L. Peng, L. Gui, X. Wang, R. Wang, D. Yu, J. Catal. 222 (2004) 493.
[16] Y. Wang, J. Ren, K. Deng, L. Gui, Y. Tang, Chem. Mater. 12 (2000) 1622.
[17] T. Hyeon, S. Lee, J. Park, Y. Chung, H. Na, J. Am. Chem. Soc. 123 (2001) 12798.
[18] X.Y. Fu, Y. Wang, N.Z. Wu, L.L. Gui, Y.Q. Tang, J. Colloid Interf. Sci. 243 (2001) 326.
[19] M. Aramendia, V. Borau, C. Jimenez, J. Marinas, F. Rodera, Bull. Soc. Chem. Jpn. 60 (1987) 3415.
[20] C. Menini, C. Park, E. Shin, G. Tavoularis, M. Keane, Catal. Today 62 (2000) 355.
[21] S. Chon, D. Allen, AIChE J. 37 (1991) 1730.